

# Real-Time Energy-Optimal Path Planning for Electric Vehicles

Saman Ahmadi\*, Guido Tack, Daniel Harabor, Philip Kilby, and Mahdi Jalili

**Abstract**—The rapid adoption of electric vehicles (EVs) in modern transport systems has made energy-aware routing a critical task in their successful integration, especially within large-scale networks. In cases where an EV’s remaining energy is limited and charging locations are not easily accessible, some destinations may only be reachable through an energy-optimal path: a route that consumes less energy than all other alternatives. The feasibility of such energy-efficient paths depends heavily on the accuracy of the energy model used for planning, and thus failing to account for vehicle dynamics can lead to inaccurate energy estimates, rendering some planned routes infeasible in reality. This paper explores the impact of vehicle dynamics on energy-optimal path planning for EVs. We develop an accurate energy model that incorporates key vehicle dynamics parameters into energy calculations, thereby reducing the risk of planning infeasible paths under battery constraints. The paper also introduces two novel online reweighting functions that allow for a faster, pre-processing free, pathfinding in the presence of negative energy costs resulting from regenerative braking, making them ideal for real-time applications. Through extensive experimentation on real-world transport networks, we demonstrate that our approach considerably enhances energy-optimal pathfinding for EVs in both computational efficiency and energy estimation accuracy.

**Index Terms**—electric vehicles, vehicle dynamics, path planning, energy-optimal paths.

## I. INTRODUCTION

THE rapid advancements in automotive and renewable energy technologies over the past decade have driven the widespread adoption of electric vehicles (EVs), solidifying their role in modern transport systems. Today, EVs are integrated into nearly all forms of transport, serving diverse purposes such as public transit with electric buses [1], daily commute with battery-powered public bikes [2], and warehouse automation with smart electric robots [3]. Although technically superior to conventional vehicles in many aspects, such as powertrain system efficiency, EVs face some challenges related to their battery capacity, slow charging process and unavailability of charging infrastructure. In scenarios where battery State of Charge (SoC) is low and charging locations are not in proximity, distant locations may only be reachable via an *energy-optimum path*, meaning a path from origin to destination that minimises energy consumption

compared to all other possible paths. It is therefore crucial to have planning algorithms that can reason about energy-optimum paths, either to calculate them directly such as in an application for satellite navigation, or as a sub-task in a bigger system such as a tool for complex vehicle routing. In transport networks, energy-optimal pathfinding is a practical real-world application of the classic shortest path problem, aiming to find the least-cost path between two locations in a network.

The quality of the energy-efficient paths critically depends on the accuracy of the energy model used to estimate the energy requirement of each road segment (link) in the underlying network. In the case of EVs, energy models must account for factors such as terrain, speed, traffic, and load to provide realistic and reliable energy predictions. While each type of EV exhibits distinct energy consumption characteristics [4], existing research often relies on energy models built based on generic vehicle categories (e.g., vehicle categories in HBEFA<sup>1</sup>) [5], [6], or simplified assumptions that do not account for system dynamics, such as focusing solely on average energy efficiency and road gradients [7], [8], [9], or assuming constant speed across road segments [10], [11], [12]. A main drawback with such simplified models is that they do not fully take vehicle dynamics into account, and thus the projected energy requirements may not reflect the actual energy required to traverse specific links in the road network. As we will see shortly, path planning with basic energy models can produce infeasible paths, where the vehicle exhausts its available energy before reaching the designated target.

### A. Case Study and Motivation

To illustrate the importance of vehicle dynamics, consider an example in Calgary, Canada, where the energy-optimal path for a round trip is planned using a basic energy model for an EV with the specifications of the *Peugeot iOn* (a sample vehicle with a 16 kWh battery capacity). We suppose there are four passengers on board and 60% initial SoC. Figure 1 shows the planned round-trip on the right, and changes in elevation and the aggregated energy consumption on the left. In this figure, we compare a conventional (basic) energy model which considers average energy consumption adjusted with road gradients (dashed red curve) with a more accurate energy model which adds vehicle load and driving patterns to the basic model (dashed green curve). The difference between the two models is 1kWh or 6.3% of the battery capacity at the end of the trip, which is clearly not negligible. More importantly, the path computed with the simpler model is

S. Ahmadi and Mahdi Jalili are with the Department of Electrical and Electronic Engineering, RMIT University, Australia. G. Tack and D. Harabor are with Monash University, Australia. P. Kilby is with Data 61 CSIRO, Australia. MJ is funded by Australian Research Council through projects DP240100963, IC240100010, IM240100042 and LP230100439. This work is also partially supported by Department of Climate Change, Energy, the Environment and Water through project number ICIRN000077.

\* saman.ahmadi@rmit.edu.au

<sup>1</sup>Handbook of Emission Factors for Road Transport, [www.hbefa.net](http://www.hbefa.net)

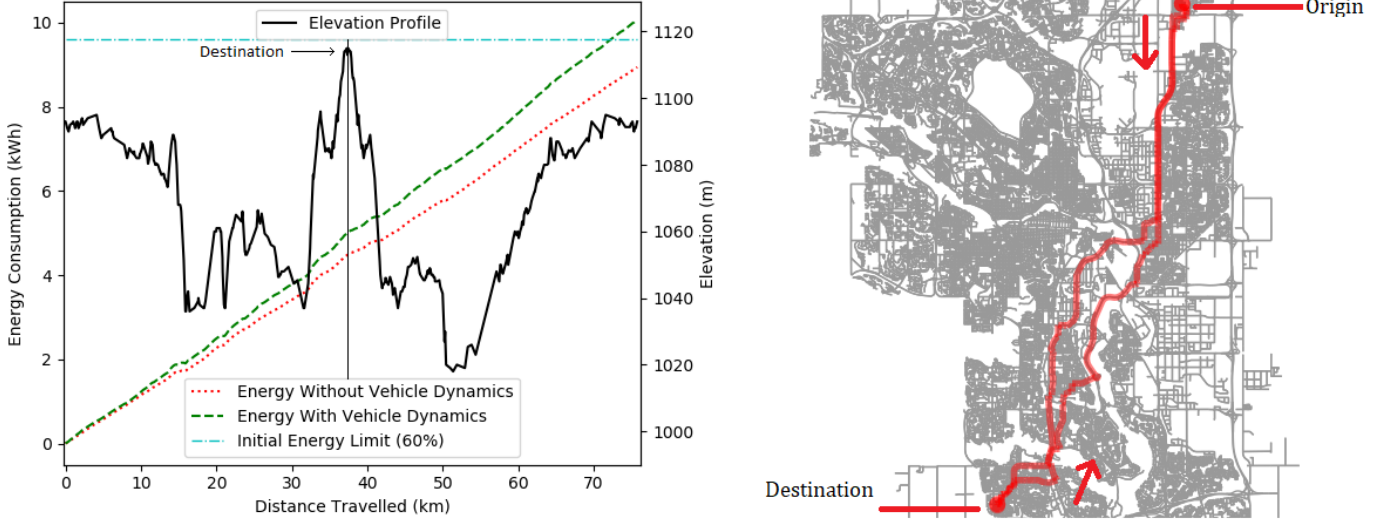


Fig. 1: [Coloured] Path, energy and elevation changes for a sample energy-efficient round-trip in Calgary.

most likely infeasible in reality, leaving the vehicle and its passengers stranded. As we will study in the experiment section, such cases are not pathological: depending on the SoC, vehicle dynamics and the length of the trip, such infeasible paths can arise in a majority of cases. We will also show that a well-designed and realistic energy model can not only improve the quality of energy estimates, but reduce the risk of producing infeasible routes, and can even yield improvements in algorithmic efficiency.

### B. Energy-optimal Pathfinding

The energy-optimal pathfinding problem aims to minimise energy consumption while ensuring route feasibility, constrained by the limited available energy. For conventional vehicles, where energy (fuel) consumption is non-negative, the problem can be efficiently solved using dynamic programming solutions such as Dijkstra’s algorithm [13]. Nonetheless, many EVs feature energy recuperation via braking, which may result in negative energy costs on some negative slopes. Baseline approaches, such as the Bellman-Ford algorithm [14], [15] are capable of solving pathfinding problems on graphs with negative weights, as in [16], [17]. However, their computational complexity is higher compared to algorithms designed for non-negative cost graphs. More recent approaches leverage the reweighting technique of Johnson’s algorithm [18] to enable more efficient pathfinding, provided the graph contains no negative cycles, a condition that is inherently satisfied in our problem due to the law of conservation of energy. In real world applications, however, we may face frequent changes either in the graphs (such as changes in the driving pattern in different traffic conditions) or in the vehicle specification (such as changes in energy consumption via varying load or number of passengers). As we will see, the overall system complexity means that without a suitable energy model and pathfinding algorithm, planned routes may indeed be infeasible in practice.

Therefore, it is crucial to have path planning algorithms that are fast and accurate in the dynamic setting.

The key contributions of this article are as follows. We first develop a data-driven energy model that accurately estimates the energy required for each road segment by incorporating key factors such as vehicle load, road gradients, and driving patterns. Algorithmically, we identify a natural characteristic of the system that allows for pre-processing free computation of energy-optimal paths via two novel reduced cost functions. While our techniques are generic, we present them in the context of EVs, as a suitable motivation for the relevance and significance of the work. For our last contribution, we investigate the impacts of vehicle dynamics on feasible energy-optimal path planning for EVs in various settings.

The remainder of this article is structured as follows. In the next section, we formally define the problem and review its classical solution approaches. In section III, we discuss vehicle dynamics and the key parameters involved in estimating EV energy consumption. Our data-driven model is presented in this section. Section IV focuses on energy-optimal pathfinding and demonstrates how our reweighing functions integrate with the core problem. Finally, in Section V, we present a comprehensive analysis of the impact of vehicle dynamics on reliable pathfinding, along with an experimental evaluation that highlights the effectiveness of our proposed model in achieving faster and more accurate pathfinding for EVs.

## II. PROBLEM FORMULATION AND BACKGROUND

Let us consider a road network modelled as a directed graph  $G = (V, E)$  with a finite set of vertices  $V$  and a set of edges  $E \subseteq V \times V$ . Each vertex  $u \in V$  corresponds to a location (intersection) and each edge  $e \in E$  corresponds to a link (road segment). A path is then defined as a sequence of vertices  $u_i \in V$  with  $i \in \{1, \dots, n\}$  such that  $(u_i, u_{i+1}) \in E$  for  $i \in \{1, \dots, n-1\}$ . Furthermore, the height function  $h : V \rightarrow \mathbb{R}^+$  returns the elevation of locations. In our

notation, expanding a typical vertex  $u$  generates a set of successor vertices, each denoted  $Succ(u)$  and we always have  $(u, Succ(u)) \in E$ . Thus, we always have  $(u, Succ(u)) \in E$ . Each edge is associated with a real-valued weight  $cost_e \in \mathbb{R}$ , which represents the amount of energy required to traverse the link. The edge costs can be retrieved via the function  $cost : E \rightarrow \mathbb{R}$ . For realistic path planning, these costs need to accurately reflect the actual energy requirement of the vehicle over the edge, and can be negative due to energy recuperation.

Assume an EV with an initial energy level of  $\mathcal{E}_{init} \in \mathbb{R}^+$  at the origin  $u_o \in V$  and with the maximum energy level of  $\mathcal{E}_{max} \in \mathbb{R}^+$  (the battery capacity). Our objective is to find an energy minimum path  $\pi^*$  from  $u_o$  to destination  $u_d \in V$  subject to the constraint that all locations on  $\pi^*$  are reached with a valid energy level in the  $[0, \mathcal{E}_{max}]$  range.

#### A. Energy Constraints and Adjustments

If standard pathfinding algorithms are used to compute minimum-energy paths without considering energy constraints, the resulting paths may consume more energy than the vehicle's battery capacity. Let  $\mathcal{E}(u) \in \mathbb{R}^+$  be the (optimal) energy level of the EV at vertex  $u$ . To ensure  $u$ 's expansion yields valid energy levels, the energy requirement of each edge  $e : (u, v)$  should be checked against two conditions during the expansion [9]. In the first case, given  $cost_e$  as the link's energy requirement, vertex  $v$  can be reached if the EV's energy level at vertex  $u$  is at least  $cost_e$ , i.e.,  $\mathcal{E}(u) \geq cost_e$ . This relation ensures feasibility via  $\mathcal{E}(v) \geq 0$  where  $\mathcal{E}(v)$  is the energy level at the end point  $v$  after traversing the edge  $(u, v)$ . The second case deals with negative cost links, and check the energy level at the end point  $v$  against the battery capacity  $\mathcal{E}_{max}$  to avoid overcharging (in the planner). If  $\mathcal{E}(v) > \mathcal{E}_{max}$ , the corresponding cost needs to be (temporarily) adjusted to limit the  $v$ 's energy level at  $\mathcal{E}_{max}$ , i.e., we set  $cost_e \leftarrow \mathcal{E}(u) - \mathcal{E}_{max}$  to have  $\mathcal{E}(v) = \mathcal{E}_{max}$ . This ensures the energy level in the planner is always capped at the maximum possible level  $\mathcal{E}_{max}$ .

#### B. Negative Weights and Graph Reweighting

In cases where the EV's energy model is not known, or so complex that it cannot be represented as a generic function, we can preprocess edge costs and convert them into non-negative values. Johnson's algorithm [18] is one such shifting method that can solve the all-pairs shortest path problem in graphs with negative costs but without negative cycles. A negative weight cycle is a cycle in which the sum of the edge costs is negative. In our application, having negative cycles means that there exists at least one cycle in our road network in which our EVs can run forever, which is not possible given the law of conservation of energy. Note that we assume no external charging happens while the EV traverses the links. Therefore, our underlying graphs contain no negative cycle, and thus the Johnson's technique [18] can be applied.

The main idea in the Johnson's method is establishing a shifting function  $\mu : V \rightarrow \mathbb{R}$  that satisfies  $cost(u, v) + \mu(u) - \mu(v) \geq 0$  for a typical edge  $(u, v) \in E$  while guaranteeing the optimality of all shortest paths when using shifted weights. It can be shown that a shifting function  $\mu$  exists if and only if the

graph has no negative cycle [18]. One such shifting function  $\mu$  can be obtained by using the Bellman-Ford [14], [15] algorithm in three simple steps: (1) add a new dummy vertex to the graph and connect it to each vertex in  $G$  with a zero-cost edge; (2) compute the shortest paths from the newly added vertex to all other vertices using the Bellman-Ford algorithm; (3) store for every vertex  $u \in V$  its optimal cost obtained during the previous step in  $\mu(u)$ , then remove the added vertex. Now, with the shifting function  $\mu$  established, one can reweight  $cost(u, v)$  to a non-negative value via  $cost(u, v) + \mu(u) - \mu(v)$ , called reduced cost function, and optimise paths for their reduced costs using the Dijkstra's algorithm, as in [7].

#### C. Related Work and Existing Solutions

Considering the state-of-the-art solutions in the literature, we can categorise the existing energy-optimal pathfinding algorithms in two approaches: (i) algorithms that traditionally establish a shifting function based on an attribute of vertices in the underlying graph, such as shifting techniques in [19] and [8]; (ii) algorithms that use a shifting function directly derived from a generic cost function, such as solutions in [10] and [12]. The former (approach i) relies on empirical costs but uses nodes' elevation to apply proper shifting, and the latter (approach ii) uses a basic energy model normally obtained by simplifying EVs' energy equations. We investigate both approaches from two aspects: their applicability to dynamic settings and the reliability of planned routes. Approach (i) is able to work with empirical energy costs or complex models, but keeping the reduced cost updated in this approach can potentially be costly in the dynamic setting as the algorithm needs to check the validity of the shifting function upon every graph change (usually in a form of preprocessing in the static mode). Therefore, this approach can offer more reliable routes, but it may not be fast enough for dynamic applications. On the other hand, approach (ii) can be adapted to be used in dynamic settings as any changes in the input parameters (and consequently output via the cost function) would simply be reflected in the shifted costs. However, the cost function is already oversimplified and does not take all the actual and realistic energy components into account. Therefore, this approach offers fast solutions to dynamic energy-optimal pathfinding, at the risk of producing infeasible routes.

We now recapitulate the state-of-the-art shifting function of [19], which works with energy and elevation data (approach i). Their height-induced potential function  $\mu_h : V \rightarrow \mathbb{R}$  is defined by  $\mu_h = \alpha h$  where  $h$  is the elevation function and  $\alpha$  is a constant factor. The value of  $\alpha$  is determined in a way that all edge costs can be safely shifted to non-negative values by ensuring  $cost(u, v) + \mu_h(u) - \mu_h(v) \geq 0$  for every edge  $(u, v) \in E$ . This is done by a linear scan of all the edges in the network during the preprocessing phase using the following strategy. For every edge  $e \in E$  with the energy requirement  $cost_e$ , we first set  $\alpha_e \leftarrow cost_e / \Delta h$  where  $\Delta h$  is the elevation difference between the link's end points. Then, if  $\Delta h > 0$  we must always have  $\alpha \leq \alpha_e$ , otherwise, if  $\Delta h < 0$  the relation  $\alpha \geq \alpha_e$  must hold. These conditions yield lower ( $\underline{\alpha}$ ) and upper ( $\bar{\alpha}$ ) bounds on the coefficient  $\alpha$ , which is non-negative in practice. Finally, we can choose any value for  $\alpha$  in

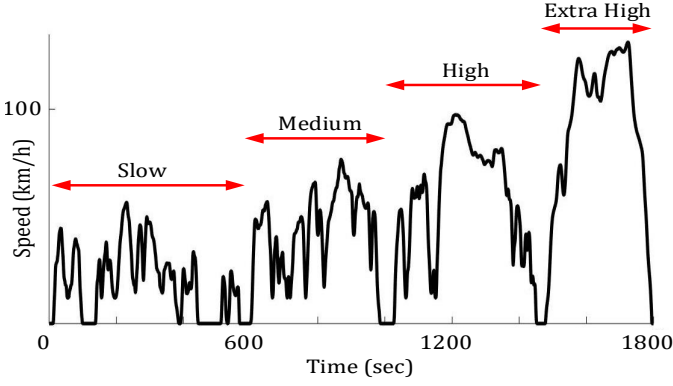


Fig. 2: The WLTP cycle and its four speed profiles [21].

the  $[\underline{\alpha}, \bar{\alpha}]$  range, where  $\underline{\alpha}$  is the largest  $\alpha_e$  among the *downhill* edges and  $\bar{\alpha}$  is the smallest  $\alpha_e$  among the *uphill* edges.

### III. VEHICLE DYNAMICS AND ENERGY EFFICIENCY

Energy-aware pathfinding for EVs requires system models that can estimate the electric energy required to traverse each road segment. In this section, we develop a novel technique that can integrate the essence of an EV's longitudinal dynamic into a cost function for energy-optimal path planning.

The energy consumption of an EV can be accurately modelled based on a so-called *longitudinal vehicle dynamics*, which essentially establishes a nonlinear relationship between the vehicle speed, mass, road gradient and the required power. Typically, the electric power drawn from the EV's energy storage system can be calculated by the following equation in a stop-and-go pattern on a non-flat road [20]:

$$P = \frac{V}{\eta} \left( Mg f_r \cos \theta + \frac{1}{2} \rho C_D A V^2 + Mg \sin \theta + M \delta \frac{dV}{dt} \right) \quad (1)$$

where  $\eta$  is the transmission efficiency,  $f_r$  is the tire rolling resistance coefficient,  $\rho$  is the air density,  $C_D$  is the aerodynamic drag coefficient,  $A$  is the frontal area of the vehicle and  $\delta$  is the coefficient of rotary elements in the vehicle. Each of these parameters can be determined empirically for any given EV, and can be considered constant in the so-called longitudinal vehicle dynamics. The remaining and interesting variables in the equation are vehicle speed  $V$ , acceleration  $dV/dt$ , mass  $M$  and the ground slope angle  $\theta$ . The values for speed and acceleration are both highly dependent on the driving pattern. One may simplify the model by assuming fixed (constant) speeds [10], [12], but, as we observed earlier in Section I, ignoring acceleration will result in inaccurate energy predictions in reality. Since the driving pattern changes with the road conditions (such as traffic congestion), predicting energy flows over trips is a difficult task. The industry-standard approach for addressing these uncertainties involves using drive cycle tests to evaluate the vehicle's energy efficiency under various driving patterns.

While several drive cycles exist for specific scenarios, we are interested in those that encompass the most prevalent driving patterns in urban transport. In this study, we utilise the WLTP<sup>2</sup> cycle, a realistic drive cycle developed from real-world

driving data. Many automotive manufacturers now report their vehicles' energy efficiency based on this standardised cycle [21]. The speed profile of WLTP and its speed categories (Slow, Medium, High, Extra-High) are depicted in Figure 2.

**Data-driven energy model:** While existing studies often rely on simplified longitudinal equations to estimate energy consumption, this research adopts a more robust, data-driven approach that integrates vehicle dynamics and road conditions, providing improved accuracy for real-world driving scenarios. Specifically, we use energy data, derived either synthetically or from real-world measurements, to build a model that maps the key vehicle dynamics variables to energy efficiency. The model development employs classic mathematical learning methods to build an explainable, high precision energy model. As we demonstrate in Section V, our experiments show that the system can be effectively represented as a quadratic cost function with high precision. Consequently, the core of our approach is an energy function that measures the energy efficiency  $cost_{ef}$  of a particular EV (usually reported in Wh/100m) under a specific driving pattern in the generic form of:

$$cost_{ef} = (ma_2 + b_2)s^2 + (ma_1 + b_1)s + (ma_0 + b_0) \quad (2)$$

Here,  $s$  is the road angle ( $\sin \theta$ ) and  $m$  is the extra mass (load/passengers' weight in kg). The coefficients  $a_i$  and  $b_i$ ,  $i \in \{0, 1, 2\}$ , are also non-negative parameters, determined by the mathematical learning method. See Table I in Section V for the range of  $a_i$  and  $b_i$  parameters for studied EVs in this paper under the speed profiles of WLTP. For synthetic data, any mathematical formulation or powertrain simulator can be employed to produce the necessary energy data for learning the energy model, provided that vehicle mass, road gradient and driving pattern can be adjusted. Our approach is versatile, allowing the model to be computed for different driving patterns. This means that the coefficients of the quadratic function above can be obtained under any driving patterns, such as the speed profiles in the WLTP cycle.

Figure 3 depicts part of our simulation results for one of our test EVs, the *Nissan Leaf*, with synthetic data. The figure shows energy efficiency in the (full) WLTP cycle with different loads and road gradients, where the initial SoC is 70%. We observe a slight yet distinct non-linear relationship between road gradient and energy efficiency. The figure also shows that the energy an EV can recuperate on a downhill slope is significantly lower than the energy required to ascend the same gradient. This imbalance is primarily due to the braking strategy and the overall system efficiency.

### IV. PATHFINDING WITH ONLINE REDUCED COSTS

This section introduces two novel online reweighting functions that allow standard energy-optimal pathfinding algorithms to establish a valid shifting function without graph reformulation. We first present our model-based approach, followed by a model-independent method.

#### A. Model-based Reduced Cost

Given the energy model of the EV provided in the form of Eq. (2), we can calculate the energy cost of edge  $e \in E$  as:

$$cost(e) = m(a_2s^2 + a_1s + a_0)l + (b_2s^2 + b_1s + b_0)l \quad (3)$$

<sup>2</sup>Worldwide Harmonised Light Vehicles Test Procedure

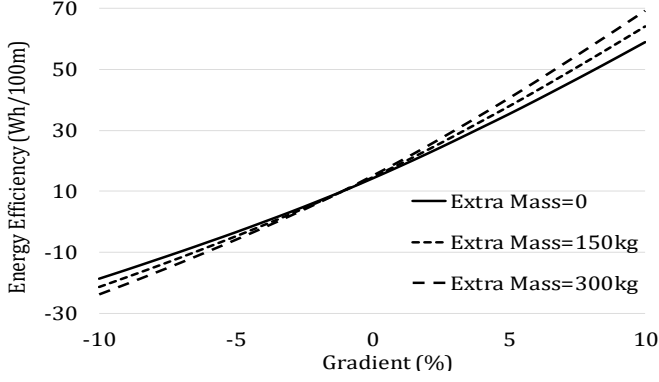


Fig. 3: Average energy efficiency for the *Nissan Leaf* over WLTP in different scenarios using synthetic data.

where  $l$  is the length of the edge  $e$  (in units of 100m). We can then develop a formula for energy consumption along path  $\pi$  with  $n$  edges. Each edge  $j \in \{1, \dots, n\}$  is characterised by its length  $l_j$  and road elevation angle  $s_j$ . The energy consumption along the path  $\pi$  can thus be formulated as

$$cost(\pi) = m \sum_{j=1}^n \sum_{i=0}^2 (a_{i,j} s_j^i) l_j + \sum_{j=1}^n \sum_{i=0}^2 (b_{i,j} s_j^i) l_j \quad (4)$$

Since each link of the path may be traversed with a different driving pattern, the parameters  $a_i$  and  $b_i$  are now also indexed by  $j$ . We observe that, since the cost function is naturally convex and all the coefficients are non-negative, the only terms that can produce negative costs are  $a_{1,j} s_j$  and  $b_{1,j} s_j$  for the links with negative ground slope, i.e.,  $s_j < 0$ . Thus, we can define the potentially negative component of the cost as:

$$cost_{neg}(\pi) = m \sum_{j=1}^n a_{1,j} s_j l_j + \sum_{j=1}^n b_{1,j} s_j l_j \quad (5)$$

Let us analyse this potentially negative component further. In [8], the authors show that when the underlying system is known, the reduced cost function can be obtained using the elevation difference if the energy function is linear. Having a nonlinear and more realistic system model, we extend that idea to find a suitable reduced cost function that fits our elevation-dependent energy model, while taking driving patterns into account. Our first observation is that  $s_j = \sin \theta_j = \Delta h_j / l_j$ , with  $\Delta h_j$  denoting the elevation difference over link  $j$ . Additionally, we can approximate the  $a_1$  and  $b_1$  coefficients using the average values of  $\bar{a}_1$  and  $\bar{b}_1$  (computed over patterns) to simplify the potentially negative portion of the path cost to

$$cost_{neg}(\pi) \approx \sum_{j=1}^n (m \bar{a}_1 + \bar{b}_1) \Delta h_j = (m \bar{a}_1 + \bar{b}_1) \Delta H \quad (6)$$

where  $\Delta H = \sum_{j=1}^n \Delta h_j$ . We can observe that the approximated energy here only depends on the elevation difference between the end points of the path, that is,  $\Delta H$ . Hence, we refer to this term as the *path-independent* component of the energy cost or  $cost_{pi}$ , which can be computed for any pair of locations as a deterministic cost. Based on this important observation, we can remove the main part of possibly negative

energy costs and obtain the reduced term as  $cost - cost_{pi}$ . For the range of energy coefficients and link gradients in road networks, we usually have  $cost \geq cost_{pi}$  which yields non-negative reduced costs. In exceptional cases with  $cost < cost_{pi}$ , we may overestimate the energy cost of the link by up to  $|cost - cost_{pi}|$  to keep the reduced cost non-negative. Our preliminary investigation shows that this situation is not easily generated in practice as the  $a_1$  and  $b_1$  coefficients across driving patterns are quite similar with a small deviation. This means that instead of link-specific values  $a_{1,j}$  and  $b_{1,j}$  for each vehicle type, we can use their average without losing much accuracy in our reduced cost function. We will investigate this approximation error (measuring cases with  $cost < cost_{pi}$ ) for the EVs of this study in the experiment section.

### B. Model-independent Reduced Cost

When detailed energy data is unavailable to derive an energy model in the form of Eq. (2), the shifting approach of [19] can still be applied to reweight the graph. This shifting function requires  $\mathcal{O}(E)$  time to compute an appropriate  $\alpha$ -value. This may be prohibitive when the network changes dynamically (e.g. when the EV specification changes), which would require  $\alpha$  to be re-calculated. To eliminate this overhead, we borrow a basic law from physics and present our model-independent reduced cost as  $cost - cost_{pot}$  with  $cost_{pot}$  denoting the change in the gravitational potential energy obtained by its classic definition in physics as

$$cost_{pot} = (M + m)g\Delta H \quad (7)$$

where  $M + m$  is the total mass of the EV (vehicle kerb mass  $M$  and additional load  $m$ ),  $g$  is the acceleration of gravity (9.8 N/kg) and  $\Delta H$  represents the height difference. Therefore, this reduced cost can be utilised in online settings, as its required parameters (elevation data and vehicle mass) are generally known or can be reasonably estimated. Since the energy requirement for each link is calculated independently, we can assert that using the potential cost function described above always results in non-negative reduced energy costs (see Appendix A for the proof).

The potential function  $cost_{pot}$  helps us to map energy costs to non-negative values without any overhead. Note that this shifting function can also be used with basic (less accurate) models where the energy cost function is established based on the aggregation of potential and kinetic energies (ignoring driving patterns), such as models in [10] and [22]. In this case, the reduced cost only contains the kinetic part of the energy, which is assumed to be non-negative.

### C. Energy-optimal Search with Reduced Costs

We now explain how our reduced cost functions can be incorporated into classic pathfinding algorithms, such as Dijkstra's algorithm, to identify energy-efficient paths. We present a pseudocode of our energy-optimal Dijkstra search with energy constraints in Algorithm 1. The algorithm starts with initialising the priority queue  $\mathcal{Q}$ , the parent array  $\mathcal{P}$ , and the arrays  $\mathcal{C}$  and  $\mathcal{E}$ , which keep track of the smallest reduced cost and available energy at each vertex, respectively. Given

---

**Algorithm 1: Energy-optimal Dijkstra Search**


---

**Inputs:** A problem instance  $(G, cost, u_o, u_d, \mathcal{E}_{init})$   
**Output:** Energy requirement of the optimal path

```

1  $\mathcal{Q} \leftarrow \emptyset$ 
2  $\mathcal{P}(u) \leftarrow \emptyset, \mathcal{C}(u) \leftarrow \infty, \mathcal{E}(u) \leftarrow -\infty$  for all  $u \in V$ 
3  $\mathcal{C}(u_o) \leftarrow 0, \mathcal{E}(u_o) \leftarrow \mathcal{E}_{init}$ 
4 Add  $u_o$  to  $\mathcal{Q}$ 
5 while  $\mathcal{Q} \neq \emptyset$  do
6   Remove from  $\mathcal{Q}$  a vertex  $u$  with the smallest  $\mathcal{C}$ -value
7   if  $u = u_d$  then break
8   foreach  $v \in Succ(u)$  do
9      $cost_e \leftarrow cost(u, v)$ 
10    if  $\mathcal{E}(u) < cost_e$  then continue
11    if  $\mathcal{E}(u) - cost_e > \mathcal{E}_{max}$  then  $cost_e \leftarrow \mathcal{E}(u) - \mathcal{E}_{max}$ 
12     $cost_{red} \leftarrow \text{Max}(0, cost_e - cost_{pi/pot}(u, v))$ 
13    if  $\mathcal{C}(u) + cost_{red} < \mathcal{C}(v)$  then
14       $\mathcal{C}(v) \leftarrow \mathcal{C}(u) + cost_{red}$ 
15       $\mathcal{E}(v) \leftarrow \mathcal{E}(u) - cost_e$ 
16       $\mathcal{P}(v) \leftarrow u$ 
17      if  $v \notin \mathcal{Q}$  then add  $v$  to  $\mathcal{Q}$ 
18 return  $\mathcal{E}_{init} - \mathcal{E}(u_d)$ 

```

---

$\mathcal{E}_{init}$  as the initial energy, the algorithm then sets the reduced cost and energy at the origin location and inserts  $u_o$  into the queue to commence the search. In every iteration of the search, the algorithm extracts from  $\mathcal{Q}$  a vertex with the smallest  $\mathcal{C}$ -value among all vertices present in the queue (line 6). Let this extracted vertex be  $u$ . If  $u$  is the destination location  $u_d$  (line 7), we can terminate the search and return  $\mathcal{E}_{init} - \mathcal{E}(u_d)$  as the energy cost of the optimum path. Otherwise, the search use  $u$ 's successors to extend the partial path. Let  $v$  be one such successor vertex. During this extension, the algorithm checks  $cost_e$  (energy requirement of the edge) against the  $\mathcal{E}(u)$  (available energy at  $u$ ) to make sure the EV has enough energy to reach the adjacent vertex (line 10), or to check whether the link's energy needs to be adjusted (line 11). The energy adjustment is only done when the EV's battery cannot fully capture the recuperated energy in some negative slopes. Then, the (always non-negative) reduced energy  $cost_{red}$  is calculated via Eq. (7) or Eq. (6) depending on the reweighting approach (line 12). Finally, if extending the current partial path via link  $(u, v)$  reaches  $v$  with a reduced cost smaller than  $\mathcal{C}(v)$ , we can update this reduced cost and insert  $v$  into the queue for further extensions (if it is not already present in  $\mathcal{Q}$ ). Note that, since traversing the link  $(u, v)$  with  $\mathcal{E}(u)$  is feasible, the available energy at the successor vertex  $v$  will be  $\mathcal{E}(u) - cost_e$ .

## V. EXPERIMENTAL ANALYSIS

This section studies the performance of our energy-optimal path planner with the proposed online reduced costs, and also investigates the impact of vehicle dynamics on the quality of energy-optimal paths planned for EVs. To evaluate our contributions within a real-world transport context, we consider road networks of six different cities with various road categories: Munich, Milan, Calgary, Canberra, Vancouver, and San Francisco. The map data was sourced from OpenStreetMap contributors<sup>3</sup> using the Python package OSMnx [23], focusing on the central area of each city. We enriched each map with

elevation and real travel time data using the *Bing*, *Mapbox* and *Here* APIs<sup>4</sup>. Average gradients are given in Table IV while network sizes can be found in Table III.

**EV simulator:** This research utilises the powertrain simulator ADVISOR (ADvance VehIcle Simulator)<sup>5</sup> to generate realistic energy data. ADVISOR uses the MATLAB engine to simulate the vehicle's powertrain using both backward (solving dynamic equations from the driving cycle to the energy source) and forward (analysing energy flow from the energy source to wheels) simulations, based on mathematical models of all components of the EV and detailed dynamic equations such as Eq. (1). Vehicle models in ADVISOR represent actual interactions between components based on input/output relationships. Blocks in ADVISOR include, but are not limited to, equations in vehicle dynamics, system efficiencies, thermal properties and extra features such as auxiliary electricity loads [24]. Therefore, it provides more accurate estimates on EVs' energy efficiency under realistic scenarios, such as driving a non-empty vehicle with the stop-and-go pattern on road segments with a positive/negative slope.

Figure 4 shows ADVISOR's high-level block diagram for EVs including the main components in the EV powertrain. The backward simulation (left-right arrows  $\rightarrow$ ) calculates the required energy to meet the given speed in the driving cycle, while the power delivered to the wheels is measured through the forward simulation (right-left arrows  $\leftarrow$ ) which is more realistic when the speed is continuously changing in different traffic conditions. More accurately, the forward simulation is a response to the backward simulation and calculates the actual amount of energy the EV's battery can supply during the provided driving cycle.

**System models and selected EVs:** We now explain how advanced engineering simulations with realistic driving can be utilised to extract accurate models in the generic form of Eq. (2). We first used the driving patterns of the WLTP cycle to generate energy efficiency data under different driving conditions (varying load and gradient) for three selected EVs: the *Nissan Leaf* (one of the best-selling EVs [25]), the *Peugeot iOn* (used in the literature, [5], [16]) and the *General Motors EVI*, a generic EV model predefined in our simulator. For each vehicle and driving pattern, we then applied the standard polynomial regression technique to learn an energy model in the form of Eq. (2) using the synthesised energy data. We obtained high precision in all the models ( $R^2 = 0.99$ ), and the coefficients of higher orders were found nearly zero. Table II presents the coefficients of the energy models learned for the selected EVs of this study under the WLTP's speed profiles.

**Graph energy costs:** Following [5], we carefully match the realistic (average) speed of every link in our road graph with one of the driving patterns in the WLTP cycle to later select a set of coefficients that best describes the energy consumption profile of our selected EV for that link. To this end, we first retrieve the average speed of the links through several online sources. Then, we compare each link's speed with the average speed of every driving pattern and choose the closest pattern

<sup>3</sup>[www.openstreetmap.org](http://www.openstreetmap.org)

<sup>4</sup>[www.bing.com](http://www.bing.com); [mapbox.com](http://mapbox.com); [developer.here.com](http://developer.here.com)

<sup>5</sup><http://adv-vehicle-sim.sourceforge.net/>



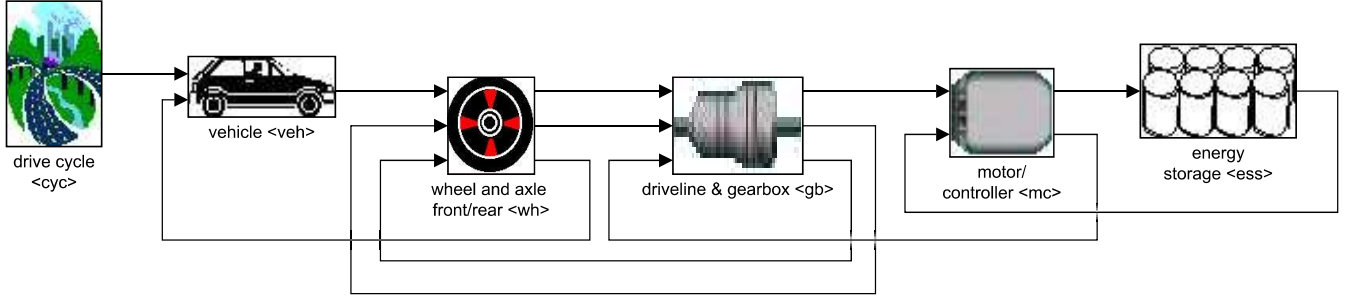


Fig. 4: EV block diagram in ADVISOR, simultaneous backward and forward simulations

TABLE I: EVs energy specifications and coefficients (in Wh/100m) over the WLTP profiles. Energy efficiency is for the entire cycle.

| Vehicle details                            | Profile   | $[a_2, a_1, a_0]$     | $[b_2, b_1, b_0]$     |
|--|-----------|-----------------------|-----------------------|
| <i>Nissan Leaf 2018</i>                    | Slow      | [0.509, 0.238, 0.004] | [671.4, 362.9, 16.12] |
| Capacity:40kWh                             | Medium    | [0.429, 0.241, 0.004] | [539.0, 370.4, 13.03] |
| Kerb weight:1544kg                         | High      | [0.472, 0.249, 0.003] | [528.2, 382.8, 12.80] |
| Efficiency:<br>$\sim 14.1 \frac{Wh}{100m}$ | ExtraHigh | [0.829, 0.283, 0.002] | [677.9, 415.4, 15.43] |
|  | Overall   | [0.595, 0.258, 0.003] | [602.5, 389.2, 14.24] |
| <i>Peugeot iOn 2017</i>                    | Slow      | [0.398, 0.244, 0.005] | [315.3, 264.7, 12.60] |
| Capacity:16kWh                             | Medium    | [0.451, 0.241, 0.004] | [381.9, 262.3, 10.04] |
| Kerb weight:1050kg                         | High      | [0.526, 0.249, 0.004] | [511.1, 259.7, 10.36] |
| Efficiency:<br>$\sim 11.5 \frac{Wh}{100m}$ | ExtraHigh | [0.731, 0.262, 0.004] | [734.5, 293.1, 13.31] |
|  | Overall   | [0.579, 0.251, 0.004] | [536.7, 272.8, 11.65] |
| <i>GM EV1</i>                              | Slow      | [0.382, 0.261, 0.005] | [505.1, 374.5, 12.44] |
| Capacity:27kWh                             | Medium    | [0.311, 0.271, 0.004] | [325.9, 388.0, 10.43] |
| Kerb weight:1450kg                         | High      | [0.485, 0.284, 0.003] | [354.5, 397.0, 10.46] |
| Efficiency:<br>$\sim 11.5 \frac{Wh}{100m}$ | ExtraHigh | [0.632, 0.291, 0.004] | [645.7, 428.9, 12.70] |
|  | Overall   | [1.473, 0.227, 0.002] | [608.3, 397.3, 11.25] |

that matches the link's average speed. The result is a realistic set of energy weights (in Wh/100m), provided in Table I. We can see that the coefficients  $a_1$  and  $b_1$  are nearly in the same range for each vehicle type. Therefore, the function  $cost_{pi}$  presented in Eq. (6) is fairly accurate.

#### A. Parametric Comparison of Approaches

Table II provides the practical range of the parameters for each pathfinding technique described in this article, including edge shifting using Johnson's algorithm  $\pi_h$ , shifting with potential energy  $cost_{pot}$  and shifting with path-independent energy  $cost_{pi}$ . The coefficients associated with  $cost_{pot}$  and  $cost_{pi}$  are vehicle-specific and fixed among networks, but the bounds on the coefficient  $\alpha$  are calculated based on the energy requirements in road networks and vary in each graph. As an example, the range of  $\alpha$  in Table II has been calculated for the given EVs operating in Calgary without any passenger or extra load. A quick look over the values in this table shows that, for every vehicle type, the coefficients  $Mg$  and  $\bar{b}_1$  are within the bounds of  $\alpha$ . Therefore, our reduced cost functions would not incur any kind of energy error. We will further investigate this in detail for different maps with varying loads.

#### B. Algorithmic Performance

Our first set of experiments evaluates the impacts of the presented reduced cost functions on the performance of energy-optimum pathfinding. For this experiment, our energy coefficients are characteristic for the *Nissan Leaf* (with details

TABLE II: Coefficients of each shifting technique (Wh/100m). Values for  $\mu_h$  are for the network of Calgary without any passenger.

| Vehicle            | Mass<br>$kg$ | $cost_{pot}$ |        | $cost_{pi}$ |             | $\mu_h$              |                |
|--------------------|--------------|--------------|--------|-------------|-------------|----------------------|----------------|
|                    |              | $g$          | $Mg$   | $\bar{a}_1$ | $\bar{b}_1$ | $\underline{\alpha}$ | $\bar{\alpha}$ |
| <i>Nissan Leaf</i> | 1544kg       | 0.273        | 421.51 | 0.253       | 382.87      | 218.18               | 541.98         |
| <i>Peugeot iOn</i> | 1050kg       | 0.273        | 286.65 | 0.249       | 269.92      | 138.60               | 388.92         |
| <i>GM EV1</i>      | 1450kg       | 0.273        | 395.85 | 0.277       | 397.09      | 275.16               | 505.42         |

shown in Table I). We assume an initial battery SoC of 70% and with three on-board passengers<sup>6</sup>. All the energy weights are obtained using our realistic energy model in Eq. (2) and we run all the algorithms on the same graph.

We compare our online reduced-cost approaches, which use Dijkstra's algorithm, with the Bellman-Ford and Johnson (edge shifting with potential functions) algorithms. For the case of shifting with  $\mu_h$ , we set  $\alpha$  to be the average of its lower and upper bounds. All algorithms were implemented in Python 3.6 using the NetworkX 2.3 package [26]. Timings are based on the average of five individual runs reported in *seconds*, running on a single core of an Intel Core i7-6700 with 3.4GHz and 16GB of RAM. Table III presents the network sizes and results for around 1,000 random (*origin, destination*) pairs as point-to-point trips using the *Nissan Leaf*. The results of the extended experiments for the other EVs of this study with different number of passengers can be found in Appendix B.

Table III gives Bellman-Ford times as a baseline. This table reports the values of parameters used in each algorithm and the runtime and pre-processing time (in seconds) separately for each algorithm. Moreover, all of the queries were solved to optimality, and we verified that all algorithms found identical solutions. Table III also shows the lower and upper bounds on the coefficient  $\alpha$  in all instances. Since the range of the graph-specific coefficient  $\alpha$  in every road network of the experiment fully covers our vehicle-specific coefficients for both  $cost_{pi}$  and  $cost_{pot}$  functions, i.e., we have  $(m + M)g \in [\underline{\alpha}, \bar{\alpha}]$  and  $(m\bar{a} + \bar{b}) \in [\underline{\alpha}, \bar{\alpha}]$ , we can ensure that there is no error associated with our reduced costs and thus the shifting process.

According to the results in Table III, the reweighting-based algorithms can significantly improve the overall run time compared to Bellman-Ford. We can see that edge sifting with  $\mu_h$  offers smaller pre-processing times to compute potentials compared to the traditional approach in the Johnson's technique. Meanwhile, our implementation of Dijkstra's algorithm

<sup>6</sup>75kg per passenger based on European Directive 95/48/EC

TABLE III: Experiment results and parameters for the *Nissan Leaf* with three passengers.

| City Network                                    | Algorithm Name         | Algorithm Parameters   | Runtime(s) |       |       |
|---|------------------------|--|------------|-------|-------|
|   |                        |  | Prep.      | Avg   | Max   |
| Munich<br>Nodes:<br>13,974<br>Arcs:<br>36,228   | Bellman-Ford           | $\alpha \in [236, 616]$<br>$mg + Mg = 483$<br>$m\bar{a} + \bar{b} = 440$ | 0.000      | 10.13 | 16.96 |
|   | Johnson                |  | 1.316      | 0.329 | 0.642 |
|   | Johnson- $\pi_h$       |  | 0.394      | 0.324 | 0.697 |
|   | Dijkstra- $cost_{pot}$ |  | 0.000      | 0.317 | 0.658 |
|   | Dijkstra- $cost_{pi}$  |  | 0.000      | 0.317 | 0.635 |
| Milan<br>Nodes:<br>13,377<br>Arcs:<br>26,539    | Bellman-Ford           | $\alpha \in [235, 616]$<br>$mg + Mg = 483$<br>$m\bar{a} + \bar{b} = 440$ | 0.000      | 6.472 | 11.69 |
|   | Johnson                |  | 1.019      | 0.249 | 0.514 |
|   | Johnson- $\pi_h$       |  | 0.285      | 0.244 | 0.533 |
|   | Dijkstra- $cost_{pot}$ |  | 0.000      | 0.239 | 0.501 |
|   | Dijkstra- $cost_{pi}$  |  | 0.000      | 0.239 | 0.474 |
| Calgary<br>Nodes:<br>32,603<br>Arcs:<br>77,172  | Bellman-Ford           | $\alpha \in [253, 615]$<br>$mg + Mg = 483$<br>$m\bar{a} + \bar{b} = 440$ | 0.000      | 24.03 | 47.33 |
|   | Johnson                |  | 3.016      | 0.693 | 1.520 |
|   | Johnson- $\pi_h$       |  | 0.802      | 0.675 | 1.467 |
|   | Dijkstra- $cost_{pot}$ |  | 0.000      | 0.665 | 1.404 |
|   | Dijkstra- $cost_{pi}$  |  | 0.000      | 0.665 | 1.419 |
| Canberra<br>Nodes:<br>23,594<br>Arcs:<br>52,112 | Bellman-Ford           | $\alpha \in [253, 615]$<br>$mg + Mg = 483$<br>$m\bar{a} + \bar{b} = 440$ | 0.000      | 12.63 | 20.12 |
|   | Johnson                |  | 2.646      | 0.466 | 1.022 |
|   | Johnson- $\pi_h$       |  | 0.571      | 0.459 | 1.001 |
|   | Dijkstra- $cost_{pot}$ |  | 0.000      | 0.451 | 1.027 |
|   | Dijkstra- $cost_{pi}$  |  | 0.000      | 0.451 | 0.964 |
| Vancouver<br>Nodes:<br>7,599<br>Arcs:<br>23,012 | Bellman-Ford           | $\alpha \in [237, 629]$<br>$mg + Mg = 483$<br>$m\bar{a} + \bar{b} = 440$ | 0.000      | 2.938 | 5.131 |
|   | Johnson                |  | 1.051      | 0.179 | 0.380 |
|   | Johnson- $\pi_h$       |  | 0.247      | 0.176 | 0.379 |
|   | Dijkstra- $cost_{pot}$ |  | 0.000      | 0.171 | 0.361 |
|   | Dijkstra- $cost_{pi}$  |  | 0.000      | 0.170 | 0.357 |
| San Fran.<br>Nodes:<br>9,555<br>Arcs:<br>26,809 | Bellman-Ford           | $\alpha \in [230, 617]$<br>$mg + Mg = 483$<br>$m\bar{a} + \bar{b} = 440$ | 0.000      | 4.505 | 9.410 |
|   | Johnson                |  | 2.582      | 0.205 | 0.486 |
|   | Johnson- $\pi_h$       |  | 0.285      | 0.198 | 0.460 |
|   | Dijkstra- $cost_{pot}$ |  | 0.000      | 0.193 | 0.474 |
|   | Dijkstra- $cost_{pi}$  |  | 0.000      | 0.193 | 0.460 |

using  $cost_{pi}$  and  $cost_{pot}$  eliminates the preprocessing phase of Johnson's and presents slightly faster execution times. It is therefore particularly useful in situations where graphs need to be updated frequently (e.g., due to changing traffic conditions).

### C. Energy-Optimum Path Analysis

Our next set of experiments investigates how vehicle dynamics affects energy-optimum paths. Here, we investigate the importance of vehicle dynamics in energy-efficient pathfinding for EVs by comparing the planned paths of different energy models. For the experimental comparison, we used three different energy models, which take vehicle dynamics into account to varying degrees. The base case in this experiment is an energy model that uses road gradients and the EV average energy efficiency, i.e.,  $cost_b = \bar{b}_2 s^2 + \bar{b}_1 s + \bar{b}_0$ . The second case adds mass as an extra parameter via  $cost_m = (m\bar{a}_2 + \bar{b}_2) s^2 + (m\bar{a}_1 + \bar{b}_1) s + (m\bar{a}_0 + \bar{b}_0)$ . The third case incorporates driving patterns only as  $cost_d = b_2 s^2 + b_1 s + b_0$  with coefficients now being link specific. The energy coefficients in these two cases are average among the patterns. Finally, the last case considers our detailed model with both mass and driving patterns, as in Eq. (2). The EV-based implementation of the Bellman-Ford algorithm was used to find energy-optimum paths for the same graphs and node pairs as in our first experiment.

Table IV shows the result of incorporating vehicle dynamics into energy-optimal pathfinding. Extra mass (vehicle load) and driving pattern (speed profiles) are the parameters for which we study the length and the required energy of the resulting optimal paths. Column  $\Delta p$  shows the percentage of paths that

are different compared to when neither vehicle load nor speed profiles of roads is taken into account. Similarly,  $\Delta l$  is the difference in path length,  $\Delta cost$  is the difference in energy consumption and  $\Delta cost_{ef}$  denotes the difference in the energy efficiency compared to the base case ( $cost_b$ ).

The results indicate that both mass and driving pattern can significantly affect energy estimates. Even when taking mass or driving pattern into account, planned routes can be up to 66% different. When adding both mass and driving patterns, the differences become larger. Interestingly, the average path length is not affected very much by solely considering vehicle load. When considering both parameters, the path length can be up to 355m longer on average (Calgary map), but for individual paths, the difference can be substantial. Figure 5 depicts two energy-optimum paths for a single (*origin, destination*) pair in each city of this experiment, where the energy-optimum path using the more accurate energy model (right) is significantly longer than the one using the basic model (left). When considering changes in energy requirements, we find maximum differences of up to 469Wh compared to the base case (Milan map). Looking at the average energy consumption values, we observe that the base model underestimates energy requirements by up to 316Wh on average (Munich map). Neglecting mass and driving patterns can also affect the estimated energy efficiency, where it can be miscalculated by up to 6.9Wh/100m (San Francisco map). This amount of miscalculation can clearly lead to the resulting trip being infeasible, depending on initial battery levels. Our next experiment will study these effects further.

### D. Feasibility Study

The third experiment of this study investigates the feasibility of routes executed without vehicle dynamics considerations. This experiment finds around 5,000 energy-optimum round-trips for random (*origin, destination*) pairs in Calgary with the *Peugeot iOn* as the test vehicle with 60% initial SoC and four passengers on board. We first find the energy-optimum path in the road network with the basic energy model (without taking mass and driving pattern into account) and then recalculate the energy requirement of the same path with our accurate energy model in which vehicle dynamics is respected.

Figure 6 focuses on the energy requirements of paths longer than 65km when different parameters of vehicle dynamics are considered. As we expected, adding mass to the energy model will increase the energy requirement of paths. Interestingly, incorporating the driving patterns may change the total energy cost in the opposite way, reducing the energy requirements on some trips. This reduction is primarily due to overestimating energy requirements on certain links along the path, where in reality, the speed profile demands less energy. Meanwhile, it is less likely to get an overestimated path when both mass and driving patterns are considered. For the random trips shown in Figure 6, the first infeasible path is observed at a distance of 69km. Of all the trips that are longer than 69km (where the first infeasible trip is observed), 44% of the routes would be infeasible if vehicle load and speed variation (driving patterns) are taken into account. Indeed, using these two parameters, all the trips with a distance of 76km and over are infeasible.



TABLE IV: Path, distance and energy differences using vehicle dynamics parameters w.r.t a model that use road gradients only.

| City          | Vehicle load | Speed profiles | $\Delta p(\%)$ | $\Delta l(m)$ |     |      | $\Delta l(\%)$ |     |      | $\Delta cost(Wh)$ |     |     | $\Delta cost_{ef}(Wh/100m)$ |     |     |
|---------------|--------------|----------------|----------------|---------------|-----|------|----------------|-----|------|-------------------|-----|-----|-----------------------------|-----|-----|
|               |              |                | Avg            | Min           | Avg | Max  | Min            | Avg | Max  | Min               | Avg | Max | Min                         | Avg | Max |
| Munich        | ●            | ○              | 1.9            | 0             | 1   | 55   | 0.0            | 0.0 | 0.5  | -1                | 81  | 191 | -0.1                        | 0.7 | 1.5 |
|               | ○            | ●              | 18.1           | -18           | 47  | 1503 | -0.2           | 0.3 | 8.2  | 2                 | 203 | 481 | 0.0                         | 1.7 | 2.3 |
|               | ●            | ●              | 18.3           | -18           | 49  | 1503 | -0.2           | 0.3 | 8.2  | 16                | 316 | 725 | 1.0                         | 2.7 | 3.3 |
| Milan         | ●            | ○              | 5.2            | 0             | 1   | 34   | 0.0            | 0.0 | 0.4  | 0                 | 53  | 130 | 0.4                         | 0.7 | 1.0 |
|               | ○            | ●              | 8.4            | 0             | 5   | 1277 | 0.0            | 0.1 | 11.1 | -2                | 141 | 309 | -0.5                        | 1.8 | 2.0 |
|               | ●            | ●              | 10.0           | 0             | 7   | 1277 | 0.0            | 0.1 | 11.1 | 0                 | 216 | 469 | 0.1                         | 2.8 | 3.0 |
| Calgary       | ●            | ○              | 6.6            | 0             | 1   | 127  | 0.0            | 0.0 | 1.2  | -30               | 142 | 417 | -0.5                        | 0.7 | 2.1 |
|               | ○            | ●              | 65.8           | -105          | 330 | 3407 | -0.6           | 1.4 | 11.4 | -150              | 121 | 471 | -1.3                        | 0.6 | 2.5 |
|               | ●            | ●              | 66.6           | -83           | 355 | 3388 | -0.5           | 1.5 | 11.4 | -22               | 300 | 795 | -0.6                        | 1.5 | 3.7 |
| Canberra      | ●            | ○              | 4.0            | 0             | 1   | 146  | 0.0            | 0.0 | 1.4  | -5                | 119 | 304 | -0.4                        | 0.7 | 2.0 |
|               | ○            | ●              | 55.8           | -82           | 224 | 2456 | -0.9           | 1.1 | 13.6 | -294              | 35  | 290 | -1.3                        | 0.3 | 2.5 |
|               | ●            | ●              | 55.9           | -82           | 240 | 2796 | -0.9           | 1.2 | 16.4 | -88               | 180 | 460 | -0.6                        | 1.2 | 3.6 |
| Vancouver     | ●            | ○              | 10.4           | 0             | 2   | 141  | 0.0            | 0.0 | 2.0  | -22               | 49  | 146 | -1.1                        | 0.8 | 3.2 |
|               | ○            | ●              | 12.1           | -75           | 4   | 302  | -1.0           | 0.0 | 4.8  | 5                 | 121 | 312 | 0.5                         | 1.9 | 3.1 |
|               | ●            | ●              | 16.4           | -50           | 5   | 313  | -0.9           | 0.1 | 4.8  | 10                | 188 | 495 | 2.1                         | 2.9 | 4.3 |
| San Francisco | ●            | ○              | 17.0           | 0             | 19  | 849  | 0.0            | 0.3 | 11.1 | -57               | 56  | 247 | -2.2                        | 0.9 | 6.9 |
|               | ○            | ●              | 16.6           | -899          | 37  | 1297 | -6.8           | 0.5 | 16.3 | 2                 | 118 | 342 | -1.0                        | 1.8 | 4.5 |
|               | ●            | ●              | 22.3           | -90           | 52  | 1297 | -1.2           | 0.7 | 16.3 | 3                 | 191 | 553 | 0.3                         | 3.0 | 6.9 |

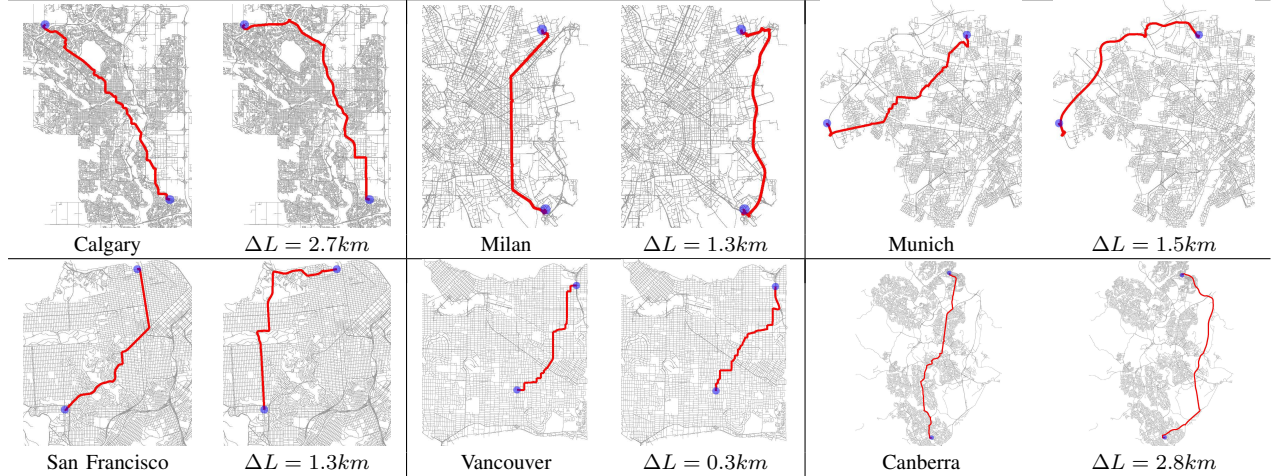


Fig. 5: Differences in the energy-optimum paths resulted by adding the parameters of vehicle dynamics. In every city, routes only based on gradient in left and routes with gradient, mass and driving patterns consideration in right.

The graph in Figure 6 (right) shows the error in energy calculation when our more accurate energy model (with vehicle load and driving pattern) is used. Analogously, trips that would consume more than initial energy (60% SoC) are infeasible. This interpretation can easily be extended to other SoC percentages. Given any initial energy level in the range of battery capacity, there always exists a path for which its energy requirement is underestimated if vehicle load and driving pattern is to be ignored. One could consider a constant factor to compensate this energy miscalculation by scaling up the estimates, but this experiment shows that, in some cases, the percentage of energy deviation can be more than 10%, a large factor when considering the full battery capacity (4kWh using *Nissan Leaf* with a battery capacity of 40kWh). Although it is true that infeasible routes may usually happen in low-battery cases, we believe that these are not corner cases. Most trips would be planned as return trips *A-B-A*, or even *multi-stop* trips, in which case even high initial SoCs may

trigger infeasibility depending on the energy capacity, as we studied through this experiment for round-trips.

#### E. Energy-time Trade-off

A typical problem of energy-optimal path planning is that minor, slow roads appear to have the lowest energy consumption and the resulting paths, therefore, take much more time than the time-optimal path, rendering them unrealistic [6]. However, when taking realistic driving patterns into account, the picture changes. According to Table I where driving patterns are considered, the simulation results show that the slow roads will in fact have relatively higher energy consumption. This means, in general, slow pattern driving on a flat road would require more energy than driving with medium or fast driving patterns. This is mainly because of multiple stop-go actions, which reduce the overall system efficiency. Consequently, energy-optimum paths using our new, more realistic energy model does not necessarily prefer slow roads. However,

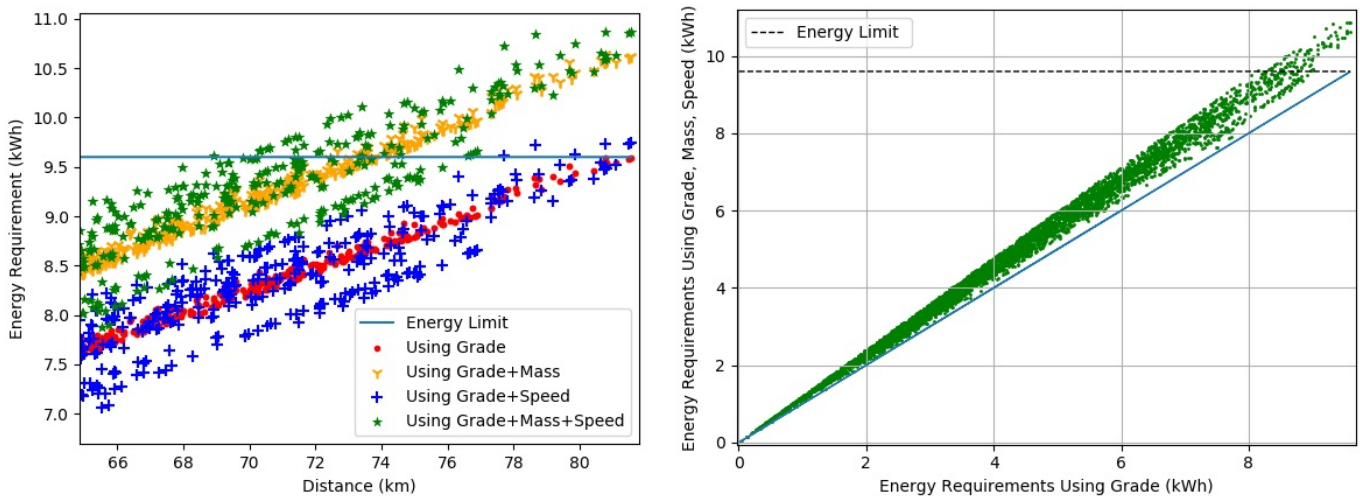


Fig. 6: [Coloured] Left: Energy versus distance (enlarged for long trips), Right: Energy deviation.

our energy-optimal paths still require a (less pronounced) trade-off between energy and time. An interesting direction for future work is to consider efficient algorithms for improving this trade-off using our nonlinear energy model, setting an upper bound on the time/distance any path can take.

## VI. CONCLUSION

This paper presents a realistic energy model for EVs based on vehicle dynamics, which not only improves the solution quality of energy-optimal pathfinding but also enables the use of pre-processing-free pathfinding algorithms. The results demonstrate that both vehicle load and driving patterns significantly influence energy estimates in path planning. Additionally, we have shown that for any initial energy level of an EV, the energy-optimal path may become infeasible if vehicle dynamics are not considered in the energy calculation. From an algorithmic perspective, we identified a natural characteristic of the system model that allows for safe reweighting of the underlying graph in the presence of negative energy costs. Furthermore, we propose an alternative reweighting approach that leverages gravitational potential energy to obtain non-negative energy costs when detailed energy data is unavailable. The nonlinear, more realistic energy model introduced in this paper can be broadly applied to standard pathfinding algorithms, using the proposed reweighting methods to achieve faster and more accurate energy-optimal pathfinding solutions.

## REFERENCES

- [1] Y. Liu and H. Liang, "A data-driven approach for electric bus energy consumption estimation," *IEEE Transactions on Intelligent Transportation Systems*, vol. 23, no. 10, pp. 17 027–17 038, 2022.
- [2] J. Zhang, W. Zhang, J. Wang, J. Feng, Z. Gao, and S. Zheng, "Rechargeable battery cabinet deployment for public bike system," *IEEE Transactions on Intelligent Transportation Systems*, vol. 23, no. 11, pp. 20 309–20 322, 2022.
- [3] A. Bolu and Ö. Korçak, "Path planning for multiple mobile robots in smart warehouse," in *7th International Conference on Control, Mechatronics and Automation, ICCMA 2019, Delft, The Netherlands, November 6-8, 2019*. IEEE, 2019, pp. 144–150. [Online]. Available: <https://doi.org/10.1109/ICCMA46720.2019.8988635>
- [4] Z. Yi and P. H. Bauer, "Optimal stochastic eco-routing solutions for electric vehicles," *IEEE Transactions on Intelligent Transportation Systems*, vol. 19, no. 12, pp. 3807–3817, 2018.
- [5] M. Baum, J. Dibbelt, T. Pajor, and D. Wagner, "Energy-optimal routes for electric vehicles," in *21st SIGSPATIAL International Conference on Advances in Geographic Information Systems, SIGSPATIAL 2013, Orlando, FL, USA, November 5-8, 2013*, C. A. Knoblock, M. Schneider, P. Kröger, J. Krumm, and P. Widmayer, Eds. ACM, 2013, pp. 54–63. [Online]. Available: <https://doi.org/10.1145/2525314.2525361>
- [6] M. Baum, J. Dibbelt, A. Gernsma, D. Wagner, and T. Zündorf, "Shortest feasible paths with charging stops for battery electric vehicles," *Transportation Science*, vol. 53, no. 6, pp. 1627–1655, 2019. [Online]. Available: <https://doi.org/10.1287/trsc.2018.0889>
- [7] S. Storandt, "Quick and energy-efficient routes: computing constrained shortest paths for electric vehicles," in *5th ACM SIGSPATIAL International Workshop on Computational Transportation Science 2011, CTS'12, November 6, 2012, Redondo Beach, CA, USA*, S. Winter and M. Müller-Hannemann, Eds. ACM, 2012, pp. 20–25. [Online]. Available: <https://doi.org/10.1145/2442942.2442947>
- [8] J. Eisner, S. Funke, and S. Storandt, "Optimal route planning for electric vehicles in large networks," in *Proceedings of the Twenty-Fifth AAAI Conference on Artificial Intelligence, AAAI 2011, San Francisco, California, USA, August 7-11, 2011*, W. Burgard and D. Roth, Eds. AAAI Press, 2011. [Online]. Available: <http://www.aaai.org/ocs/index.php/AAAI/AAAI11/paper/view/3637>
- [9] A. Artmeier, J. Haselmayr, M. Leucker, and M. Sachenbacher, "The shortest path problem revisited: Optimal routing for electric vehicles," in *KI 2010: Advances in Artificial Intelligence, 33rd Annual German Conference on AI, Karlsruhe, Germany, September 21-24, 2010. Proceedings*, ser. Lecture Notes in Computer Science, R. Dillmann, J. Beyerer, U. D. Hanebeck, and T. Schultz, Eds., vol. 6359. Springer, 2010, pp. 309–316. [Online]. Available: [https://doi.org/10.1007/978-3-642-16111-7\\_35](https://doi.org/10.1007/978-3-642-16111-7_35)
- [10] M. Sachenbacher, M. Leucker, A. Artmeier, and J. Haselmayr, "Efficient energy-optimal routing for electric vehicles," in *Proceedings of the Twenty-Fifth AAAI Conference on Artificial Intelligence, AAAI 2011, San Francisco, California, USA, August 7-11, 2011*, W. Burgard and D. Roth, Eds. AAAI Press, 2011. [Online]. Available: <http://www.aaai.org/ocs/index.php/AAAI/AAAI11/paper/view/3735>
- [11] A. Cela, T. Jurik, R. Hamouche, R. Natowicz, A. Reama, S.-I. Niculescu, and J. Julien, "Energy optimal real-time navigation system," *IEEE Intelligent Transportation Systems Magazine*, vol. 6, no. 3, pp. 66–79, 2014.
- [12] L. Shen, H. Shao, T. Wu, W. H. Lam, and E. C. Zhu, "An energy-efficient reliable path finding algorithm for stochastic road networks with electric vehicles," *Transportation Research Part C: Emerging Technologies*, vol. 102, pp. 450–473, 2019.
- [13] E. W. Dijkstra, "A note on two problems in connexion with graphs," *Numerische Mathematik*, vol. 1, pp. 269–271, 1959. [Online]. Available: <https://doi.org/10.1007/BF01386390>

- [14] R. Bellman, "On a routing problem," *Quarterly of applied mathematics*, vol. 16, no. 1, pp. 87–90, 1958.
- [15] L. R. Ford Jr, "Network flow theory," Rand Corp Santa Monica Ca, Tech. Rep., 1956.
- [16] C. De Cauwer, W. Verbeke, J. Van Mierlo, and T. Coosemans, "A model for range estimation and energy-efficient routing of electric vehicles in real-world conditions," *IEEE Transactions on Intelligent Transportation Systems*, vol. 21, no. 7, pp. 2787–2800, 2020.
- [17] F. Morlock, B. Rolfe, M. Bauer, and O. Sawodny, "Time optimal routing of electric vehicles under consideration of available charging infrastructure and a detailed consumption model," *IEEE Transactions on Intelligent Transportation Systems*, vol. 21, no. 12, pp. 5123–5135, 2020.
- [18] D. B. Johnson, "Efficient algorithms for shortest paths in sparse networks," *J. ACM*, vol. 24, no. 1, pp. 1–13, 1977. [Online]. Available: <https://doi.org/10.1145/321992.321993>
- [19] M. Baum, J. Dibbelt, T. Pajor, J. Sauer, D. Wagner, and T. Zündorf, "Energy-optimal routes for battery electric vehicles," *Algorithmica*, vol. 82, no. 5, pp. 1490–1546, 2020. [Online]. Available: <https://doi.org/10.1007/s00453-019-00655-9>
- [20] M. Ehsani, Y. Gao, S. Longo, and K. Ebrahimi, *Modern electric, hybrid electric, and fuel cell vehicles*. CRC press, 2018.
- [21] B. Ciuffo, A. Maratta, M. Tutuianu, K. Anagnostopoulos, G. Fontaras, J. Pavlovic, S. Serra, S. Tsiakmakis, and N. Zacharof, "Development of the worldwide harmonized test procedure for light-duty vehicles: Pathway for implementation in european union legislation," *Transportation Research Record*, vol. 2503, no. 1, pp. 110–118, 2015.
- [22] Y. Wang, J. Jiang, and T. Mu, "Context-aware and energy-driven route optimization for fully electric vehicles via crowdsourcing," *IEEE Trans. Intell. Transp. Syst.*, vol. 14, no. 3, pp. 1331–1345, 2013. [Online]. Available: <https://doi.org/10.1109/TITS.2013.2261064>
- [23] G. Boeing, "OSMnx: New methods for acquiring, constructing, analyzing, and visualizing complex street networks," *Computers, Environment and Urban Systems*, vol. 65, pp. 126–139, 2017.
- [24] S. Ahmadi, S. Bathaee, and A. H. Hosseinpour, "Improving fuel economy and performance of a fuel-cell hybrid electric vehicle (fuel-cell, battery, and ultra-capacitor) using optimized energy management strategy," *Energy Conversion and Management*, vol. 160, pp. 74–84, 2018.
- [25] M. Singer, "Consumer views on plug-in electric vehicles—national benchmark report," National Renewable Energy Lab.(NREL), Golden, CO (United States), Tech. Rep., 2016.
- [26] A. Hagberg, P. Swart, and D. S. Chult, "Exploring network structure, dynamics, and function using networkx," Los Alamos National Lab.(LANL), Los Alamos, NM (United States), Tech. Rep., 2008.

## APPENDIX A TECHNICAL PROOF

*Lemma.* The function  $cost - cost_{pot}$  always yields non-negative energy costs.

*Proof.* EVs may exhibit negative energy costs only on negative slopes, while the energy requirement on positive gradients is always positive. Note that a negative gradient link may still have a positive energy cost, e.g., due to friction or acceleration.

First, consider link 1 in Figure 7 with a positive slope. If the EV traverses this link, its relative height will increase by  $\Delta h_1$ . In other words, the EV will have a greater gravitational potential energy at the end node of the link. Based on the law of conservation of energy, the change in one form of energy (potential energy here) is compensated by the other form (electrical energy). Therefore, the EV must at least consume  $cost_{pot}$  to compensate the gravitational energy over uphill links, i.e.,  $cost \geq cost_{pot}$  or  $cost - cost_{pot} \geq 0$ . Therefore, the reduced cost is non-negative for the uphill edges.

Second, consider links with negative ground slopes, for example, link 2 in Figure 7. For this link, since the relational change in the height ( $\Delta h_2$ ) of the EV decreases, the gravitational potential energy is thus negative or  $cost_{pot} < 0$ . Let us

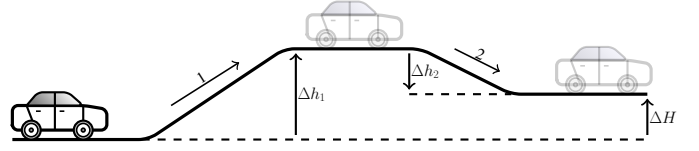


Fig. 7: A sample scenario for an EV traversing links with different gradients where  $\Delta H = \Delta h_1 + \Delta h_2$ .

assume the most optimistic scenario where the EV does not need to consume any kind of electrical energy for propulsion and has enough capacity to store the recuperated energy. In this condition, since the energy is transformed from the potential to electrical form, the maximum amount of energy the EV can regenerate by gliding on a negative slope is again limited by the gravitational potential energy, i.e.  $cost_{pot} \leq cost$  or  $cost - cost_{pot} \geq 0$ . Therefore, the reduced cost is also non-negative for the downhill edges.

Third, let us assume that  $cost$  of a link needs to be adjusted to  $cost'$  to meet the battery limits. Since we never reduce  $cost$  via the adjustment, we have  $cost \leq cost'$  which yields  $cost' - cost_{pot} \geq 0$  based on the both cases above.  $\square$

## APPENDIX B EXTENDED EXPERIMENTS

TABLE V: Experiment results and parameters for the *Peugeot iOn* without any passenger.

| City Network                        | Algorithm Name         | Algorithm Parameters       | Runtime(s) |       |       |
|-------------------------------------|------------------------|----------------------------|------------|-------|-------|
|                                     |                        |                            | Prep.      | Avg   | Max   |
| Munich Nodes: 13,974 Arcs: 36,228   | Bellman-Ford           |                            | 0.000      | 12.59 | 22.59 |
|                                     | Johnson                |                            | 1.435      | 0.375 | 0.738 |
|                                     | Johnson- $\pi_h$       | $\alpha \in [139, 387]$    | 0.416      | 0.369 | 0.738 |
|                                     | Dijkstra- $cost_{pot}$ | $mg + Mg = 287$            | 0.000      | 0.360 | 0.725 |
|                                     | Dijkstra- $cost_{pi}$  | $m\bar{a} + \bar{b} = 270$ | 0.000      | 0.359 | 0.738 |
| Milan Nodes: 13,377 Arcs: 26,539    | Bellman-Ford           |                            | 0.000      | 8.546 | 14.74 |
|                                     | Johnson                |                            | 1.104      | 0.303 | 0.592 |
|                                     | Johnson- $\pi_h$       | $\alpha \in [138, 391]$    | 0.303      | 0.276 | 0.574 |
|                                     | Dijkstra- $cost_{pot}$ | $mg + Mg = 287$            | 0.000      | 0.270 | 0.550 |
|                                     | Dijkstra- $cost_{pi}$  | $m\bar{a} + \bar{b} = 270$ | 0.000      | 0.269 | 0.547 |
| Calgary Nodes: 32,603 Arcs: 77,172  | Bellman-Ford           |                            | 0.000      | 32.43 | 61.06 |
|                                     | Johnson                |                            | 3.794      | 0.821 | 1.927 |
|                                     | Johnson- $\pi_h$       | $\alpha \in [139, 389]$    | 1.097      | 0.796 | 1.869 |
|                                     | Dijkstra- $cost_{pot}$ | $mg + Mg = 287$            | 0.000      | 0.782 | 1.851 |
|                                     | Dijkstra- $cost_{pi}$  | $m\bar{a} + \bar{b} = 270$ | 0.000      | 0.783 | 1.882 |
| Canberra Nodes: 23,594 Arcs: 52,112 | Bellman-Ford           |                            | 0.000      | 16.92 | 30.09 |
|                                     | Johnson                |                            | 2.486      | 0.461 | 0.991 |
|                                     | Johnson- $\pi_h$       | $\alpha \in [139, 391]$    | 0.595      | 0.453 | 1.000 |
|                                     | Dijkstra- $cost_{pot}$ | $mg + Mg = 287$            | 0.000      | 0.438 | 0.991 |
|                                     | Dijkstra- $cost_{pi}$  | $m\bar{a} + \bar{b} = 270$ | 0.000      | 0.438 | 0.941 |
| Vancouver Nodes: 7,599 Arcs: 23,012 | Bellman-Ford           |                            | 0.000      | 4.020 | 6.945 |
|                                     | Johnson                |                            | 1.033      | 0.191 | 0.434 |
|                                     | Johnson- $\pi_h$       | $\alpha \in [138, 391]$    | 0.269      | 0.188 | 0.430 |
|                                     | Dijkstra- $cost_{pot}$ | $mg + Mg = 287$            | 0.000      | 0.184 | 0.427 |
|                                     | Dijkstra- $cost_{pi}$  | $m\bar{a} + \bar{b} = 270$ | 0.000      | 0.184 | 0.434 |
| San Fran. Nodes: 9,555 Arcs: 26,809 | Bellman-Ford           |                            | 0.000      | 6.272 | 14.48 |
|                                     | Johnson                |                            | 2.545      | 0.223 | 0.516 |
|                                     | Johnson- $\pi_h$       | $\alpha \in [139, 391]$    | 0.312      | 0.216 | 0.503 |
|                                     | Dijkstra- $cost_{pot}$ | $mg + Mg = 287$            | 0.000      | 0.210 | 0.482 |
|                                     | Dijkstra- $cost_{pi}$  | $m\bar{a} + \bar{b} = 270$ | 0.000      | 0.210 | 0.484 |

TABLE VI: Experiment results and parameters for the *GM-EVI* with only one passenger.

| City Network  | Algorithm Name         | Algorithm Parameters       | Runtime(s) |       |       |
|---------------|------------------------|----------------------------|------------|-------|-------|
|               |                        |                            | Prep.      | Avg   | Max   |
| Munich        | Bellman-Ford           |                            | 0.000      | 13.12 | 22.77 |
| Nodes: 13,974 | Johnson                |                            | 2.137      | 0.421 | 0.955 |
| Arcs: 36,228  | Johnson- $\pi_h$       | $\alpha \in [286, 531]$    | 0.628      | 0.414 | 0.945 |
|               | Dijkstra- $cost_{pot}$ | $mg + Mg = 416$            | 0.000      | 0.404 | 0.857 |
|               | Dijkstra- $cost_{pi}$  | $m\bar{a} + \bar{b} = 418$ | 0.000      | 0.405 | 0.873 |
| Milan         | Bellman-Ford           |                            | 0.000      | 8.693 | 15.07 |
| Nodes: 13,377 | Johnson                |                            | 1.672      | 0.326 | 0.782 |
| Arcs: 26,539  | Johnson- $\pi_h$       | $\alpha \in [278, 540]$    | 0.450      | 0.319 | 0.724 |
|               | Dijkstra- $cost_{pot}$ | $mg + Mg = 416$            | 0.000      | 0.310 | 0.760 |
|               | Dijkstra- $cost_{pi}$  | $m\bar{a} + \bar{b} = 418$ | 0.000      | 0.310 | 0.732 |
| Calgary       | Bellman-Ford           |                            | 0.000      | 27.94 | 50.27 |
| Nodes: 32,603 | Johnson                |                            | 3.860      | 0.738 | 1.662 |
| Arcs: 77,172  | Johnson- $\pi_h$       | $\alpha \in [289, 532]$    | 0.901      | 0.716 | 1.509 |
|               | Dijkstra- $cost_{pot}$ | $mg + Mg = 416$            | 0.000      | 0.701 | 1.513 |
|               | Dijkstra- $cost_{pi}$  | $m\bar{a} + \bar{b} = 418$ | 0.000      | 0.700 | 1.466 |
| Canberra      | Bellman-Ford           |                            | 0.000      | 16.97 | 32.24 |
| Nodes: 23,594 | Johnson                |                            | 4.063      | 0.471 | 1.175 |
| Arcs: 52,112  | Johnson- $\pi_h$       | $\alpha \in [286, 538]$    | 0.663      | 0.464 | 1.091 |
|               | Dijkstra- $cost_{pot}$ | $mg + Mg = 416$            | 0.000      | 0.452 | 1.035 |
|               | Dijkstra- $cost_{pi}$  | $m\bar{a} + \bar{b} = 418$ | 0.000      | 0.452 | 1.049 |
| Vancouver     | Bellman-Ford           |                            | 0.000      | 3.930 | 7.642 |
| Nodes: 7,599  | Johnson                |                            | 1.925      | 0.247 | 0.567 |
| Arcs: 23,012  | Johnson- $\pi_h$       | $\alpha \in [284, 552]$    | 0.353      | 0.241 | 0.572 |
|               | Dijkstra- $cost_{pot}$ | $mg + Mg = 416$            | 0.000      | 0.236 | 0.546 |
|               | Dijkstra- $cost_{pi}$  | $m\bar{a} + \bar{b} = 418$ | 0.000      | 0.236 | 0.548 |
| San Fran.     | Bellman-Ford           |                            | 0.000      | 6.343 | 16.66 |
| Nodes: 9,555  | Johnson                |                            | 5.563      | 0.276 | 0.684 |
| Arcs: 26,809  | Johnson- $\pi_h$       | $\alpha \in [284, 541]$    | 0.435      | 0.264 | 0.660 |
|               | Dijkstra- $cost_{pot}$ | $mg + Mg = 416$            | 0.000      | 0.258 | 0.653 |
|               | Dijkstra- $cost_{pi}$  | $m\bar{a} + \bar{b} = 418$ | 0.000      | 0.258 | 0.645 |